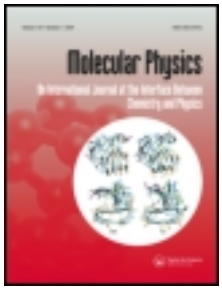

Molecular Physics: An International Journal at the Interface Between Chemistry and Physics
Publication details, including instructions for authors and subscription information:
http://www.tandfonline.com/loi/tmph20

Ultra miniature resonators for electron spin resonance: Sensitivity analysis, design and construction methods, and potential applications

Ygal Twig [a], Ekaterina Dikarov [a] & Aharon Blank [a]
[a] Schulich Faculty of Chemistry, Technion - Israel Institute of Technology, Haifa, Israel
Accepted author version posted online: 09 Jan 2013.Version of record first published: 30 Jan 2013.

To cite this article: Ygal Twig , Ekaterina Dikarov & Aharon Blank (2013): Ultra miniature resonators for electron spin resonance: Sensitivity analysis, design and construction methods, and potential applications, Molecular Physics: An International Journal at the Interface Between Chemistry and Physics, DOI:10.1080/00268976.2012.762463

To link to this article: http://dx.doi.org/10.1080/00268976.2012.762463

Molecular Physics, 2013
http://dx.doi.org/10.1080/00268976.2012.762463

Ultra miniature resonators for electron spin resonance: Sensitivity analysis, design and construction methods, and potential applications

Ygal Twig, Ekaterina Dikarov and Aharon Blank*

Schulich Faculty of Chemistry, Technion – Israel Institute of Technology, Haifa 32000, Israel

(*Received 6 November 2012; final version received 20 December 2012*)

This paper describes a recently developed new family of miniature surface resonators, used for electron spin resonance spectroscopy and imaging. The first part of the paper provides a detailed description of the operational principles of the surface resonators. It also includes sensitivity analysis for a variety of configurations with inner dimensions ranging from 150 μm down to 2 μm, operating at the Ku, Q, and W frequency bands. Most of the data presented here is based on theoretical predictions; however, some of it is accompanied by experiential results for verification. The second part of the paper describes a new type of double-surface microresonator and its production method. This new configuration enables an efficient coupling of the microwave energy from millimetre-sized microstrip lines to micron structures even at relatively low frequencies. The resonator is analysed both theoretically and experimentally – exhibiting ultra-high spin sensitivity. The conclusion of the two parts of the paper is that micron-scale surface microresonators may achieve spin sensitivity of a few thousands of spins in one second of acquisition time for special samples, such as phosphorous-doped ^{28}Si, at cryogenic temperatures. However, further miniaturization below 1–2 microns does not seem to be beneficial, sensitivity-wise. In addition to their high spin sensitivity, these resonators have a huge conversion factor, reaching in some cases to more than 500–1000 G of microwave magnetic field with input power of 1 W. Some possible applications of these unique capabilities are also described herein.

Keywords: EPR; ESR; microresonators; imaging; sensitivity

1. Introduction

Many of the problems in contemporary physical science require the observation and manipulation of a small number of electron spins, ideally even one single spin. To name just a few: (a) paramagnetic defects, impurities and dopants in semiconductors affecting solar cells and electronic devices' properties [1]; (b) small numbers of spin-labelled macromolecules used for *in-cellular* structural biology studies [2]; (c) spintronic systems [3]; and (d) electron spin-based quantum computing devices [4]. These and other similar challenges can potentially be addressed by high-sensitivity electron spin resonance (ESR) spectroscopy and imaging techniques [5]. Recent work has shown that drastically reducing the resonator's size (while trying to maintain its quality factor, Q, at reasonable high values) is a good approach to improving spin sensitivity [6–8]. As a result, unique types of surface loop-gap microresonators with an inner diameter as small as $\sim$20 μm were developed [9]. Recently, these structures achieved state-of-the-art electron spin sensitivity of $\sim 10^4$ spins for >1 hour of averaging time using a unique sample of P-doped ^{28}Si, at static fields of $\sim$0.5 T and cryogenic temperatures [10].

In the present work we show that by further reducing the size of the resonators and working at higher static fields, it is possible to push further the spin sensitivity capabilities of induction-detection ESR. However, we found that there is a practical limit to this size reduction (at a given frequency of operation), mainly due to issues of efficient coupling of the microwave (MW) signal in/out of the resonator. This was resolved here to some extent by employing a new double-sided resonator design.

In the following pages, we first present a general theoretical analysis that discusses the relevant factors affecting the spin sensitivity of surface loop-gap microresonators, such as their physical size, operating temperature, and the static magnetic field. Some theoretical predictions are given for specific representative resonator configurations at Ku-, Q-, and W-band frequencies ($\sim$16, 34 and 95 GHz). Whenever possible, the theoretical predictions are compared to the available experimental data. Following this, we provide a detailed description and some experimental data regarding our so-called 'third-generation surface resonators' that are double-sided and thus allow coupling to very small structures. (The 'first' and 'second' generations were described in Refs. [11] and [9], respectively.)

2. Surface loop-gap microresonators – general sensitivity analysis

In this section we will provide a detailed analysis of the sensitivity of surface loop-gap microresonators [9–11] as

*Corresponding author. Email: ab359@tx.technion.ac.il

a function of their dimensions, resonance frequency, and temperature of operation. It should be noted that a somewhat similar treatment was presented in the past in the context of **purely dielectric ring resonators** [7,12]. The previous multi-frequency sensitivity analysis was verified by our room temperature experiments at frequencies of ~9, 17, and up to 35 GHz [5,13]. However, many unknowns regarding low-temperature operation conditions, such as actual experimental noise and the spins' relaxation times, made the previous analysis too optimistic at cryogenic temperatures. Furthermore, the dimensions of dielectric resonators (unlike metallic surface resonator) are dictated by the materials' permittivity and the required resonance frequency, which facilitate the use of analytical methods to reach closed-form expressions. In addition, the quality factor of the high permittivity dielectrics degrades quickly as a function of frequency, which makes these materials unattractive for use at frequencies above ~35–60 GHz. It is therefore evident that a fresh analysis, focusing on the new configuration of surface loop-gap microresonators, is warranted. This analysis will be based on numerical calculations of resonator properties as well as recent experimental results and relaxation times measured at various temperatures. It will provide insights about the parametric behaviour of these types of structures in a wide range of temperatures (from 300 down to 10 K) and frequencies (from 10 up to 95 GHz), along with realistic estimations of their ESR sensitivity.

We start the analysis by looking at a typical surface loop-gap microresonator structure (Figure 1). The resonator can be considered as made of a conductive 'loop' and a 'gap' section, both supported by a dielectric material substrate (not shown in Figure 1). A basic requirement for the design process and also for sensitivity analysis is to know the resonance frequency of these types of structures, the quality factor, and the microwave fields' distribution. Very rough approximations for the resonance frequency can be found by using the expressions developed for three-dimensional loop-gap resonators [14]. These can result in typical deviations of up to a factor of 2–4 from the actual resonance frequency of our 2D structures [11], so in practice a detailed numerical finite element analysis must be employed to obtain the resonance frequency of the surface resonator presented here. The same argument holds for the calculation of the microwave fields' distribution in the resonator, which is necessary to evaluate the sample's 'filling factor' and the resonator's 'effective volume' (see below and in Refs. [6] and [15]). They cannot be evaluated in an analytical manner and have to be calculated numerically. The quality factor is even harder to evaluate since numerical methods are often not very good predictors for it and it is necessary to rely on experimental data on similar structures to come up with numbers of fair accuracy. It is therefore evident that general analytical expressions of the sort we obtained for the purely dielectric resonators [7,12] are not practical for the surface loop-gap structures, and that the latter should rather be examined in a case-by-case manner that would enable reasonable extrapolation to similar configurations.

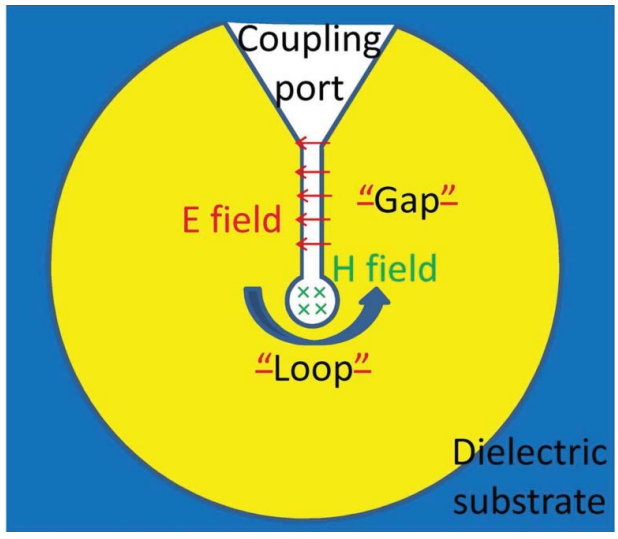

Figure 1. Schematic representation of a typical surface loop-gap microresonator. The resonator is made of a thin metallic deposition (blue) on top of a dielectric substrate (not shown). The microwave energy is coupled through the coupling port that has a strong E-field that continues into the gap area. The microwave current at resonance (marked by the curved blue arrow) goes around the loop section, generating a strong H-field inside it. The loop and the gap can be seen as an inductor and a capacitor at resonance, although the accurate description of this structure is more complicated due to its distributed nature.

The general expression for pulsed ESR spin sensitivity to be used in our analysis is taken from our previous work [11]:

$$\text{Sensitivity}_{\sqrt{\text{Hz}}}^{\text{spins}} \approx \frac{8\sqrt{V_c}\sqrt{k_b T(1/\pi T_2^*)}}{\mu_B \omega_0 \sqrt{2\mu_0}} \sqrt{\frac{\omega_0}{Q_u}} \sqrt{T_1} B_F, \quad (1)$$

where V_c represents the resonator's effective volume [6,15], which is equal to the volume of a small hypothetical sample V_v (for example $[1\ \mu\text{m}]^3$, usually located at the point where the resonator's microwave magnetic field is maximal), divided by the filling factor [16] of this small sample. The term k_b is the Boltzmann constant, T is the temperature in which the experiment is carried out (assumed to be the same for the spins and the resonator), and $(1/\pi T_2^*) = \Delta f$ is the bandwidth of signal acquisition, chosen to match the spin-spin relaxation time (including static inhomogeneities), T_2^*. The variable ω_0 is the Larmor angular frequency, Q_u is the unloaded quality factor of the resonator (including resonator and sample losses (when relevant) but excluding losses due to coupling in/out of the resonator), T_1 is the spin-lattice relaxation time, B_F is the Boltzmann population factor, $B_F = \frac{1+e^{-\frac{\hbar\omega_0}{k_B T}}}{1-e^{-\frac{\hbar\omega_0}{k_B T}}}$, μ_B is Bohr's magneton, and μ_0 is the free space permeability. It should be noted that

analogous expressions for pulsed ESR sensitivity appear in the literature [15,17,18]. Our expression in Equation (1) (developed in Refs. [5–7] and [11]) closely follows the original derivation by Mims, but without getting into the details of exciting just part of the ESR spectrum (i.e. we assume full spectral excitation). Moreover, we employ the principle of reciprocity, common in pulsed NMR literature [19], to obtain more simplified expressions. Equation (1) provides us with the parametric behaviour of the resonators' sensitivity. Thus, as we shall see, by having a range of theoretical predictions and some experimental results for a variety of surface resonator structures at a given frequency, temperature, and sample characteristics, it is possible to extrapolate in order to find the predicted sensitivity at different frequencies, temperatures, or samples, for other smaller or larger surface resonators from the same family.

We shall start our actual analysis by examining a series of structures with geometries as shown in Figure 2, designed to operate at the Ku-band (∼12–18 GHz) range. The two upper resonators (Figure 2(a) and (b)) are representative of our 'first-generation' surface resonators [11], where coupling to the microstrip line was not optimal since they did not include a coupling port (Figure 1). The middle row in Figure 2(c) and (d) features our 'second-generation' resonators, having a much smaller inner size and improved coupling [9,10]. The structures in the bottom row (Figure 2(e) and (f)) represent our newest 'third-generation' resonators with an even smaller size, which will be described in the next section in detail. They employ a double resonator structure to enable coupling to such small volumes. For each structure in Figure 2, we have calculated the resonance frequency, quality factor, and conversion factor (linking the excited microwave power to the microwave B_1 field in the resonator), both at room temperature and at 10 K. The differences between the temperatures are manifested through the larger permittivity of the rutile single crystal (i.e. 110 instead of 85 for the (001) plane and 240 instead of 165 along the crystal's C-axis), and the higher conductivity of the copper deposition (5×10^{10} instead of 5×10^{7} S/m). The results of these finite element calculations are summarized in Table 1, which also lists the calculated spin sensitivity (based on Equation 1) for two typical samples at room temperature (E′ centres in SiO_2) and at 10 K (phosphorous-doped $^{28}Si - {}^{28}Si{:}P$). We considered the relaxation times of $T_2{}^* = 100$ ns and $T_1 = 200$ μs for the SiO_2 sample, and $T_2{}^* = 800$ ns and $T_1 = 10$ μs for the $^{28}Si{:}P$ sample. The last entry in the table provides the calculated signal-to-noise ratio (SNR) for 1 second of acquisition time, for a typical 100 μM of frozen nitroxide solution at 50 K that is placed on the resonator (we assumed $T_2 = 2$ μs, $T_2{}^* =$ 10 ns, and $T_1 = 100$ μs). This SNR calculation uses Equation (4) in Ref. [11], with an additional integration over the sample volume, weighted by the factor $B_1^2/B_1^{\max 2}$. Table 1 also provides, when possible, the measured data about the resonators' characteristics and their actual measured spin sensitivity.

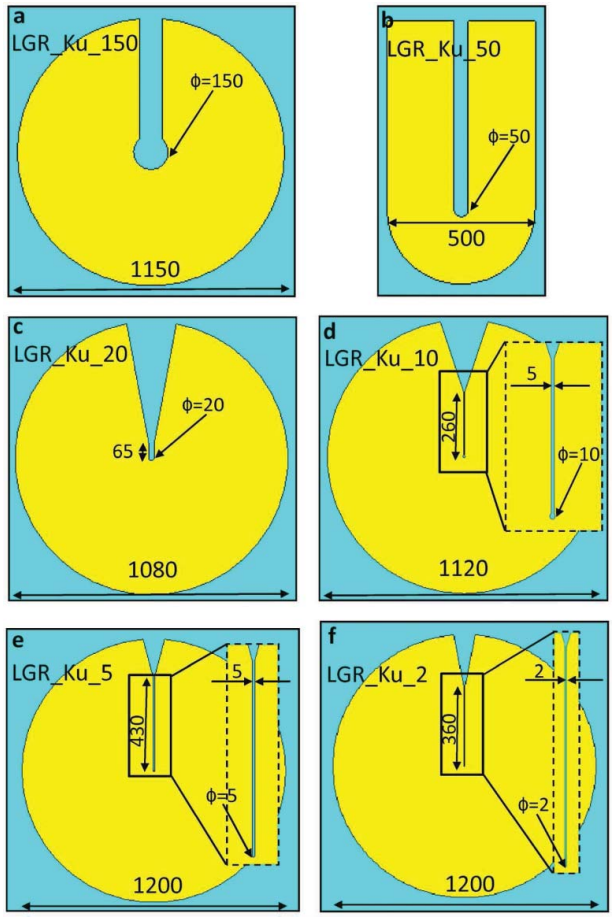

Figure 2. Physical layout and dimensions of a variety of Ku-band surface resonators, printed on a rutile single crystal. The name of each resonator appears near its drawing, and is related to the structure's inner diameter. The LGR_5 and the LGR_2 resonators represent the upper print of a double-stacked resonator structure (Figure 4) where the bottom part is LGR_20. All dimensions are in microns.

We also examined other resonator configurations at higher frequencies with the aim of further improving spin sensitivity. The resonator designs operating at Q band are shown in Figure 3(a)–(c). The design principles are the same as for the previously described resonators; however, the substrate is made out of a 200-μm-thick single crystal of $LaAlO_3$, which is an isotropic low-loss dielectric material with permittivity of 23.98 at room temperature and ∼23.7 at 10 K [20]. The reasons for using a crystal with permittivity lower than that of rutile are to maintain resonator dimensions similar to those used in the Ku band, to enable efficient coupling from the microstrip, and to avoid large changes in resonance frequency due to temperature (since our Q-band system has a limited bandwidth of ∼33–37 GHz). We have calculated the microwave fields' distribution for each structure in Figure 3(a)–(c), and a representative

Table 1. Calculated and measured properties of Ku-band surface loop-gap microresonators (see Figure 2 for resonator names and dimensions).

Name of structure	LGR_Ku_150	LGR_Ku_50	LGR_Ku_20	LGR_Ku_10	LGR_Ku_5	LGR_Ku_2
V_c [nL] [1]	6.9	4.5	0.37	0.18	0.093	0.042
V_w [μm × μm × μm] [2]	∼120 × 120 × 10	∼50 × 100 × 10	∼20 × 60 × 4	∼10 × 150 × 3	∼5 × 150 × 3	∼2 × 120 × 2
Calc. (meas.) f_0 RT [GHz] [3]	12.72 (12.36)	13.74 (–)	16.93 (17.05)	17.52 (–)	16.59 (15.76)	19.45 (–)
Calc. (meas.) f_0 LT [GHz] [4]	10.36 (–)	12.25 (–)	14.44 (14.25)	15.28 (–)	14.29 (–)	16.9 (–)
Calc. (meas.) Q_u RT [5]	56 (15)	68 (–)	23 (15)	26 (–)	40 (51)	30 (–)
Calc. (meas.) Q_u LT [6]	240 (–)	200 (–)	80 (200)	60 (–)	56 (–)	52 (–)
Calc. (meas.) conv. factor RT [G/$\sqrt{W}$] [7]	45 (86)	80 (–)	157 (–)	170 (–)	565 (300)	630 (–)
Calc. (meas.) conv. factor LT [G/$\sqrt{W}$] [8]	52 (–)	90 (–)	170 (134)	376 (–)	690 (–)	1250 (–)
Calc. (meas.) sens. RT (E′ in SiO_2) [Spins/$\sqrt{Hz}$] [9]	1.2×10^9 (3.1×10^8)	7.4×10^8 (–)	2.6×10^8 (–)	1.7×10^8 (–)	1.0×10^8 ($3 \times 10^{7)}$	6.4×10^7 (–)
Calc. (meas.) sens. LT (^{28}Si:P) [Spins/$\sqrt{Hz}$] [10]	3.6×10^5 (–)	2.1×10^5 (–)	8.6×10^4 (3.4×10^5)	6.5×10^4 (–)	5.3×10^4 (–)	2.9×10^4 (–)
Calc. nitroxide SNR, 50 K [SNR/$\sqrt{Hz}$] [11]	601	580	88	62	15	13

[1]The effective volume [6,15] as defined in the text.
[2]Rough estimate of the working volume where the magnetic energy is larger than its maximum value divided by 2. Dimensions are given along the horizontal, vertical and out-of-plane axes centered on the resonator's centercentre. This parameter is useful to estimate the instantaneous field of view observed by the resonator when a sample is placed on it.
[3]The calculated (measured – when available) resonance frequency at room temperature.
[4]The calculated (measured – when available) resonance frequency at 10 K.
[5]The calculated (measured – when available) unloaded quality factor at room temperature.
[6]The calculated (measured – when available) unloaded quality factor at 10 K.
[7]The calculated (measured – when available) microwave rotating frame B_1 in the resonator for 1 W of input power at room temperature.
[8]The calculated (measured – when available) microwave rotating frame B_1 in the resonator for 1 W of input power at 10 K.
[9]The calculated (measured – when available) spin sensitivity for a sample of γ-irradiated SiO_2 at room temperature.
[10]The calculated (measured – when available) spin sensitivity for a sample of phosphorous-doped ^{28}Si at 10 K.
[11]The calculated SNR for 100 μM of a typical frozen nitroxide solution at 50 K.

example is provided in Figure 4(a). The results for the calculated properties of these three Q-band structures appear on the left-hand side of Table 2. This family of resonators has not been fabricated yet. The plan for operating these resonators relies on excitation via a microstrip line, similar to the Ku-band resonators. The microstrip is excited via a thin 0.86 mm semi-rigid coaxial line through a simple adaptor (see [10]), which itself is connected to a WR-28 waveguide via waveguide-to-coax adapter. A similar scheme was used to excite our purely dielectric resonators at Q band [5].

For the high end of expected sensitivity performance we looked at the possibility of constructing W-band surface resonators that operate at ∼95 GHz. Here we made use of a single crystal with even lower permittivity, i.e. sapphire (Al_2O_3), which is anisotropic and, just like rutile, has one axis with a larger permittivity of 11.45, compared to the permittivity in the plane perpendicular to it, which is 9.4 [20]. The geometry of the W-band resonators is shown in Figure 3(d)–(f). It was calculated with a sapphire substrate thickness of 150 μm; the results of the calculations appear in Table 3. The resonators LGR_W_20 and LGR_W_5 were fabricated at the Technion's clean room facility with a 200-μm-thick sapphire substrate. Figure 5(a) shows an optical microscope photo of one of the manufactured LGR_W_20 resonators. In order to allow coupling without significant losses along the transmission line, coming and going from the microwave bridge, we produced a special circular-to-microstrip waveguide transition and used a special microstrip line made of 150-μm-thick quartz with gold plating. The transition is based on the down-scaling in size (up-scaling in frequency) of the design presented in Ref. [21] for 9–11 GHz. At W band we managed to obtain a bandwidth of 12 GHz (∼86–98) for this transition, verified by vector network analyser measurements (Anritsu, model 37397) using a two-port symmetric transition system (Figure 5(b)). Following that, we cut the two-port system along its symmetry plane and measured the one-port response of the LGR_W_20 and LGR_W_5 resonators by placing them at the most optimal location (coupling-wise) along the microstrip line, as schematically depicted in Figure 5(c). Typical results exhibiting clear resonance (with Q of ∼12) centred at ∼88 GHz are shown in Figure 5(d).

3. Third-generation surface loop-gap microresonators: design, production method, and experimental results

Following this general description and mainly theoretical analysis of various resonator configurations, we want to focus now on a specific experimental example of our most

Table 2. Calculated and measured properties of Q- and W-band surface loop-gap microresonators (see Figure 3 for resonator names and dimensions).

Name of structure	LGR_Q_20	LGR_Q_5	LGR_Q_2	LGR_W_20	LGR_W_5	LGR_W_2
V_c [nL]	0.50	0.10	0.10	0.31	0.14	0.11
V_w [μm × μm × μm]	~20 × 20 × 5	~8 × 6 × 3	~2 × 15 × 1.5	~20 × 20 × 4	~8 × 26 × 1.8	~4 × 15 × 1.2
Calc. f_0 RT [GHz]	34.58	33.70	34.47	95.0 [1]	95.1 [1]	94.8
Calc. f_0 LT [GHz]	34.82	33.99	34.7	95.0	95.1	94.8
Calc. Q_u RT	87	71	76	50 [2]	48 [2]	45
Calc. Q_u LT	107	96	96	61	50	48
Calc. conv. factor RT [G/$\sqrt{W}$]	226	430	471	67	92	125
Calc. conv. factor LT [G/$\sqrt{W}$]	245	539	548	90	109	132
Calc. sens. RT (E′ in SiO_2) [Spins/$\sqrt{Hz}$]	5.47×10^7	2.8×10^7	2.6×10^7	1.2×10^7	8.5×10^6	7.8×10^6
Calc. sens. LT (^{28}Si:P) [Spins/$\sqrt{Hz}$]	2.35×10^4	1.2×10^4	1.1×10^4	5.5×10^3	4.1×10^3	3.7×10^3
Calc. nitroxide SNR, 50 K[SNR/$\sqrt{Hz}$]	84	49	38	401	260	225

[1]Measured frequency of 89 GHz of a slightly different configuration (see Figure 5).
[2]Measured unloaded Q of ~24 (see Figure 5).

recent 'third-generation' resonators. In previous works [6,8–11], and also in this paper's theoretical Section II it was made clear that, in order to improve spin sensitivity, it is necessary to reduce the resonator's size as much as possible while still maintaining reasonable values of the quality factor, Q (which would justify calling it a 'resonator'). The smallest size we reached in our previous work was a surface resonator with inner dimensions of ~20 × 65 μm (see Figure 2(c)) for operation in the Ku-band range (~14–17 GHz, depending on the temperature) [9,10]. While smaller designs can be calculated and constructed for the Ku band, they run into the problem of efficiently coupling the microstrip line to the resonator (Figure 6(a)). Namely, in such small resonators, microwave energy is concentrated in a very small volume; therefore, it essentially hinders all coupling efforts from the millimetre-scale microstrip line to the micron-scale resonator. One way to overcome this is to move into higher frequencies, as was

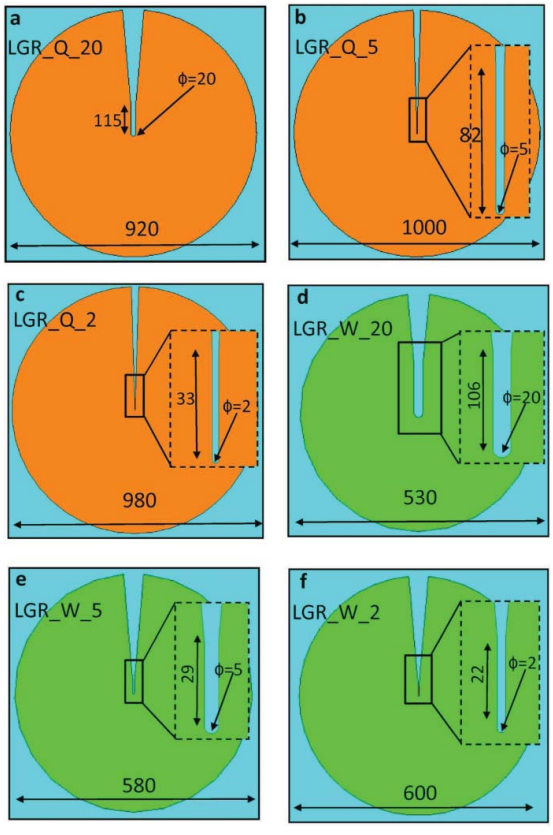

Figure 3. Physical layout and dimensions of a variety of Q- and W-band surface resonators. The inserts in Plates b–f show the fine details of the inside of the resonators. All dimensions are in microns.

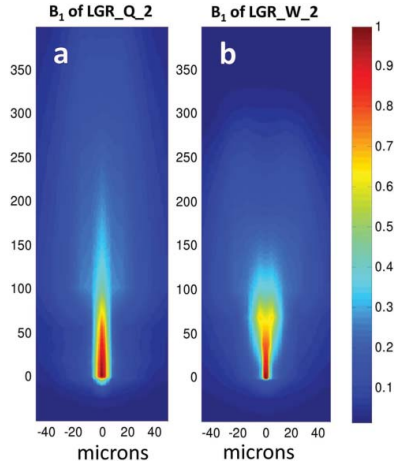

Figure 4. Calculated microwave magnetic field for two typical Q- and W-band resonators (LGR_Q_2 on the left and LGR_W_2 on the right) in a plane located 2.5 μm above the resonator's surface. The colour bar shows the field values normalized to the maximum field in the plane.

Table 3. Preparation protocol for two-sided surface loop-gap microresonators (LGR_5 and LGR_2).

Surface preparation	Wafer type: TiO_2
	Cleaning: ultrasonic bath in acetone, methanol and isopropanol (5 min each). Final rinse with water.
	Heating: on plate at 300°C for 10 min
Photoresist coating	Photoresist type: Clariant AZ 5214 E
	Spin velocity: 1500 rpm
	Spin time: 1 min
Pre-Bake	On a hotplate at 110°C for 90 sec
Exposure	System: Karl Suss MA-6 Mask Aligner
	Exp. type: Soft contact
	Alignment gap: start with 35 μm and eventually bring to full contact
	Exp. time: 1.9 sec
Post-Bake	On a hotplate at 120°C for 2 min
Flat exposure	Exposure without mask on mask aligner for 15 sec
Development	Total development time: 45 sec
Metal deposition	System: Airco Temescal FC-1800 E-beam evaporator
	First layer: Ti (100 A°)
	Second layer: Au (9000 A°)
Lift-off	Ultrasonic bath in acetone for 5 min
Si_3N_4 deposition	System: PlasmaTherm -790 PECVD
	Gases: SiH_4/N_2 and NH_3
	Temperature: 250C. Time: 17 min
	Layer thickness: 3000A

Note: The process on the other side of the TiO_2 crystal is the same, except for the need to align the resonators using alignment marks during the exposure process.

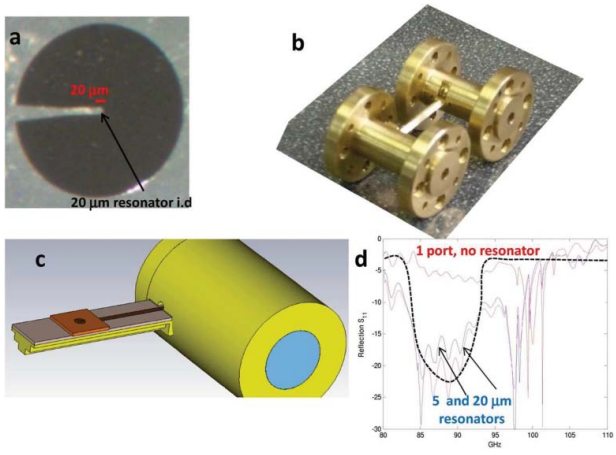

Figure 5. Preliminary results for a surface microresonator at 88 GHz. (a) Optical image of the resonator. (b) Photo of the waveguide-to-microstrip transitions used for the two-port measurements, and then one-port measurements (after cutting it at the centre). (c) Drawing of the one-port structure used for testing the resonator. (d) Reflection coefficient of the coupling line without resonators (red) and with resonators with an i.d. of 5 μm (blue) and 20 μm (magenta). A resonance mode with loaded $Q_L \sim 12$ is clearly visible, but because of the low Q there are many reflections and small dips inside the large resonance mode caused by small line reflections (the dashed black line serves as a guide to the eye).

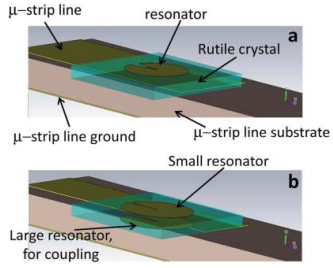

Figure 6. Coupling schemes to the surface loop-gap microresonators. (a) 'Conventional' one-stage coupling to the resonator of interest. (b) A two-stage gradual coupling scheme to a relatively large lower resonator, which is coupled to a smaller resonator of interest on top of the rutile crystal.

demonstrated above. However, we wanted to provide a more general solution that would also make it possible to further decrease resonator size in all frequency bands in the future. To the end of solving the coupling problem, we came up with the hybrid design depicted in Figure 6(b). This new resonator is made of two metallic parts that sandwich the dielectric substrate. The lower part is made of our previous $\sim 20 \times 65$-μm resonator (LGR_Ku_20), which is designed to have the same resonance frequency as the upper resonator. The latter can now be much smaller than previous designs and still couple well to the microstrip line through the lower resonator. Thus, this structure can be described as a non-symmetric double-stacked loop-gap surface microresonator. We will proceed to make a theoretical and experimental analysis of such structures featuring upper resonators of two different sizes, with inner diameters of 5 and 2 μm.

Figure 7 shows the details of one of the upper resonators with an inner diameter of 5 μm (LGR_Ku_5) and Figure 8(a) and (b) shows its calculated electric and magnetic fields. Other relevant properties of this and of the 2-μm resonator are presented in Table 1. The magnetic microwave energy is clearly concentrated at the centre of the resonator and along the boundaries of the thin gap. Figure 8(c) shows that both the lower and upper resonators are excited at the same frequency, but that the field is much stronger for the upper (smaller) one.

The resonators were manufactured at the Technion's clean room facility using the lithographic process detailed in Table 3. Following these processes, the rutile crystal with several identical resonators was sliced using a diamond blade and a single resonator was fitted onto our cryogenic ESR imaging probe [10] to perform actual measurements in our home-made pulsed ESR system [5]. The experiments reported here were carried out only at room temperature and employed a test sample of γ-irradiated quartz (i.e. E′ centres in SiO_2) with $\sim 4 \times 10^{16}$ defects per cubic centimetre (measured by Bruker's EMX CW system with respect to a reference sample). We employed a simple Hahn echo sequence with interpulse delay of $\tau = 1000$ ns and

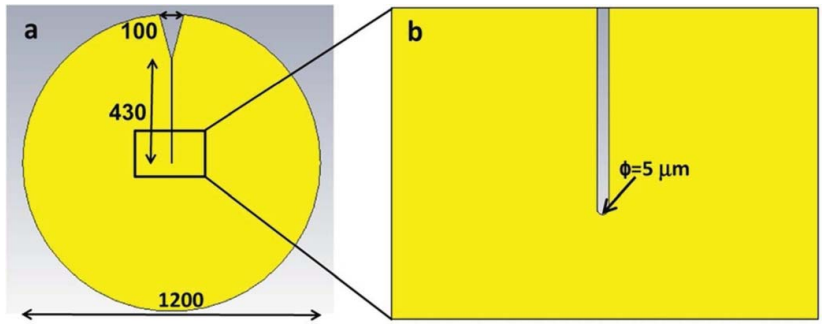

Figure 7. Physical dimensions of the LGR_Ku_5 resonator (in microns). (a) A large-scale view of the resonator, with the yellow part representing a 1-μm copper layer deposited on a 200-μm-thick rutile single crystal (with the crystal's C-axis horizontal). The bottom part of the crystal has the old 20 × 65-mm resonator [10] patterned on it (not shown here, only in Figure 1(b)). (b) Enlarged view of the centre of the resonator.

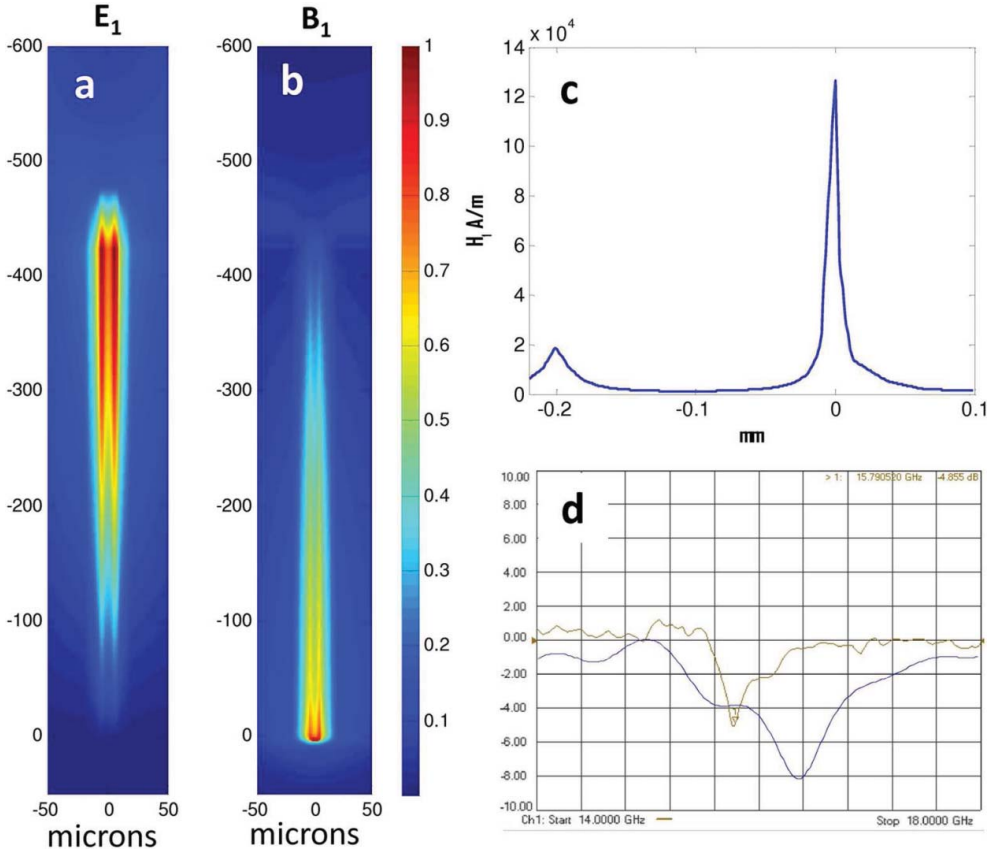

Figure 8. (a) Electric (marked as E_1) and (b) magnetic (marked as H_1) fields, as calculated by the finite-element microwave simulation, for the LGR_Ku_5 resonator around its central feature (1 μm above the copper surface). The origin is at the centre of the resonator. (c) The B_1 field plotted at the centre of the resonator along a line going out-of-plane from −220 μm (below the surface of the resonator) up to 100 μm above it. The incident microwave power going into the resonator that was considered in these calculations is 1 W. (d) Calculated (blue line) and measured (brown line) reflection coefficient (S_{11}) of the LGR_Ku_5 resonator.

$\pi/2$ (π) pulse lengths of 30 (60) ns, with a repetition rate of 5 kHz. The time-domain echo signal of this measurement is shown in Figure 9, along with the noise (recorded under the same conditions but at a 100-G field offset). The measured spin sensitivity was evaluated using the known sample's spin concentration and the calculated microwave magnetic fields of the resonator, as described in [11]. Briefly, although the sample is much larger than the resonator and extends well into areas where there is no B_1 field, our numerical calculations allow us to know the actual volume from which the signal is acquired. Basically, this is done by summing all voxel elements in the sample and weighing their contribution to the signal according to the local value of $B_1^2/B_1^{\max 2}$.

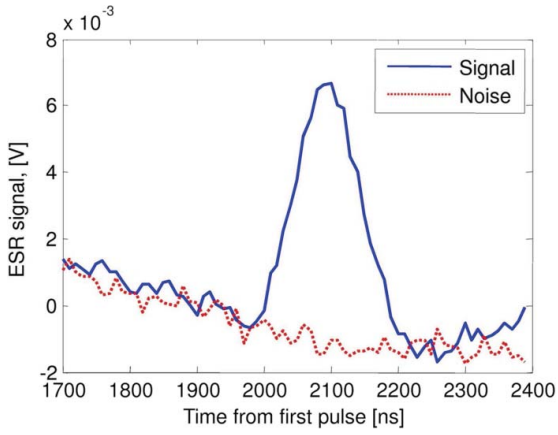

Figure 9. A time-domain ESR signal of γ-irradiated SiO_2 measured with the LGR_Ku_5 resonator at room temperature. The signal (solid blue line) and noise (dashed red line) were both reordered with 48,000 averages (∼10 s at 5 kHz repetition rate).

4. Discussion

Surface loop-gap microresonators have proved to be the most sensitive configuration employed to date in induction-detection ESR. This is due to their record-breaking small effective volume (while maintaining reasonable high Q values, especially at low temperatures), which, based on Equation (1), is the major factor facilitating their high sensitivity. Here we examined (mainly theoretically) configurations that go down to an inner diameter size of 2 μm and show a steady increase in sensitivity as we move from larger to smaller sizes. In principle, it is possible to imagine reaching much smaller structures, in the hundreds or tens of nanometres, made available by modern lithographic methods. In practice, however, regarding our family of resonators, this means having a longer 'gap' that requires an increased capacitance in order to compensate for the reduction in 'loop' inductance (and thus maintain a fixed resonance frequency). This is not desirable since the microwave magnetic field also spreads out to parts of the gap (see Figures 4 and 8), which implies that such further considerable miniaturization would generate very small benefits, if any at all – as is apparent from our calculations. Having a small loop and a relatively long gap also means that the Q of the resonator (which is proportional to loop inductance) becomes smaller – a trend shown in Tables 1 and 2. The bottom line of all of this is that further miniaturization does not seem to be beneficial, sensitivity-wise. For example, there is not much gain in spin sensitivity when going from LGR_Ku_10 to LGR_Ku_5 or when moving from LGR_Q_5 to LGR_Q_2 and also from LGR_W_5 to LGR_W_2, as apparent in Tables 1 and 2 (LGR_Ku_2 shows quite an improvement with respect to LGR_Ku_5, but this is mainly because it was designed for a higher frequency). Furthermore, coupling to the microstrip can become a problem because, even with the double-stacked configuration, there is a limit to the difference in size between the lower and upper resonators that would still support efficient coupling to the smaller one. Finally, a much smaller loop size means that the sensitive volume extends to a very small height above the resonator. Already in the 2-μm resonators the sample must be very close (∼1.5 μm) to the resonator's surface to enable good measurements; therefore, much smaller loop sizes would mean that, in practice, the sample must be grown or placed directly on the resonator – which can be very challenging. The limited set of experimental results we presented provides good support for our theoretical analysis. These results, together with the above-mentioned insights about the prospects of further miniaturization, make it evident that the configurations presented here represent the current upper limit for this surface resonator technology. Therefore, the resonators presented in this work represent a viable approach to the further improvement of induction-detection spin sensitivity by a factor of ∼23 by advancing from the configuration described in the recent work with the LGR_Ku_20 resonator operating at Ku band [9,10] to the future LGR_W_2 resonator operating at W band. We have begun to travel along this path, and have already reached nice sensitivity levels at room temperature for the LGR_Ku_5 resonator. Also, we have achieved a basic design and measured MW properties for the LGR_W_5 resonator.

The characteristics of the resonant structures presented here, such as spin sensitivity, quality, and conversion factor, can be compared to some relevant data from the literature for especially small loop-gap resonators. For example, Forrer and co-workers describe a cryogenic loop-gap resonator with a volume of ∼40 nL, operating at Q band, with a room-temperature Q factor of 205, that has a conversion factor of 17 G/$\sqrt{}$W (but the absolute spin sensitivity is not reported) [22]. Hyde and co-workers present two miniature loop-gap and TE011 resonators at W band, only to find out that at these frequencies the latter, with a volume of ∼71 nL, shows the better results [23]. These include a Q factor of 2380, conversion factor of ∼30 G/$\sqrt{}$W, and spin sensitivity of $\sim 2 \times 10^9$ spin/$\sqrt{}$Hz for liquid samples at room temperature. It is thus apparent that the performance of 'conventional' miniature loop-gap and cylindrical resonators is quite distant from that of the surface resonators presented here, although their Q factor is better. Another example from the literature, which is of relevance, is the use of surface *microstrip-based* resonators [8]. Some of these structures were already analysed and compared to our structures in a previous paper [11]. Here we note that the smallest of those microstrip resonators, with typical dimension of ∼20 μm at ∼14 GHz, showed a Q factor of ∼55, conversion factor of ∼200 G/$\sqrt{}$W, and absolute spin sensitivity of $\sim 10^9$ spin/$\sqrt{}$Hz at room temperature for a DPPH sample [8]. These capabilities are somewhat inferior to those presented here but still represent a viable approach to resonator miniaturization. The main limiting issues with these resonators are the lack of variable coupling

capability and the need for a physically large impedance matching stub, which limits the lower value of the resonator's volume.

Finally, an important issue that needs some discussion is related to the possible applications of the loop-gap surface resonators presented here. As noted in the introduction, there are many subjects in science that require the measurement of a small number of spins and could benefit from these new types of resonators. However, the virtues of the surface resonators presented here go far beyond mere spin sensitivity. One important issue, for example, is the high conversion factor that facilitates the excitation of large spectral bandwidths using reduced microwave power. For example, the LGR_Q_5 resonator has a conversion factor of more than 500 G/$\sqrt{}$W, which means that a $\sim$1 GHz bandwidth could be excited by a 1-ns MW hard pulse with a power of less than 1 W. The relatively low Q of the surface resonators also supports such instantaneous large bandwidths of excitation and short dead time. Such capability can be very useful for many modern two-dimensional ESR spectroscopic techniques. One potential example of this is double quantum coherence (DQC) for measuring the distance between two spin labels [24]. These measurements, which are commonly carried out at 50–100 μM spin concentrations, find it difficult to excite an entire broad spectrum of common nitroxides (50–100 G), and certainly seem impractical for spin labels with even broader spectra (e.g. Gd^{3+} [25]). The use of surface microresonators can provide good results for such applications and allow for good sensitivity even with small sample volumes, as is apparent from the last row in Tables 1 and 2. Other potential applications are related to microimaging [6] and diffusion [26] and stem from the high spin sensitivity of these resonators, as well as from the ability to place gradient coils very close to the sample without affecting the resonator's properties (and thus to produce very large gradients with relatively small current pulses).

Acknowledgements

This work was partially supported by grant #213/09 from the Israeli Science Foundation, grant #201665 form the European Research Council (ERC), and by the Russell Berrie Nanotechnology Institute at the Technion. We acknowledge Dr. Graham Smith and his team from St. Andrews for their help with the network analyser measurements at W band. The help and support of Arkady Gavrilov and Avshalom Shai from the Technion's Micro-Nano Fabrication Unit are greatly appreciated.

References

[1] G.D. Watkins, Phys Solid State **41** (5), 746 (1999).
[2] T.F. Prisner, I. Krstic, R. Hansel, O. Romainczyk, J.W. Engels, and V. Dotsch, Angew Chem Int Edit **50** (22), 5070 (2011).
[3] D.D. Awschalom and N. Samarth, Physics **2**, 50 (2009).
[4] V. Cerletti, W.A. Coish, O. Gywat, and D. Loss, Nanotechnology **16** (4), R27 (2005).
[5] L. Shtirberg, Y. Twig, E. Dikarov, R. Halevy, M. Levit, and A. Blank Rev. Sci. Instrum. **82** (4), 043708 (2011).
[6] A. Blank, C.R. Dunnam, P.P. Borbat, and J.H. Freed, J. Magn. Reson. **165** (1), 116 (2003).
[7] A. Blank and J. H. Freed, Isr. J. Chem. **46** (4), 423 (2006).
[8] R. Narkowicz, D. Suter, and I. Niemeyer, Rev. Sci. Instrum. **79** (8), 084702 (2008).
[9] Y. Twig, E. Dikarov, W.D. Hutchison, and A. Blank, Rev. Sci. Instrum. **82** (7), 076105 (2011).
[10] Y. Twig, E. Dikarov, and A. Blank, J. Magn. Reson. **218**, 22 (2012).
[11] Y. Twig, E. Suhovoy, and A. Blank, Rev. Sci. Instrum. **81** (10), (2010).
[12] A. Blank, in *Multifrequency Electron Paramagnetic Resonance, Theory and Applications*, edited by S.K. Misra (Wiley-VCH, Berlin, 2011).
[13] A. Blank, E. Suhovoy, R. Halevy, L. Shtirberg, and W. Harneit, Phys. Chem. Chem. Phys. **11** (31), 6689 (2009).
[14] S.S. Eaton, G.R. Eaton, and L.J. Berliner, *Biomedical EPR*. (Kluwer Academic/Plenum Publishers, New York, 2004).
[15] W.B. Mims, in *Electron Paramagnetic Resonance*, edited by S. Geschwind (Plenum Press, New York, 1972), Chap. 4, p. 263.
[16] C.P. Poole, *Electron Spin Resonance: A Comprehensive Treatise on Experimental Techniques*, 2nd ed. (Wiley, New York, 1983).
[17] P.P. Borbat, R.H. Crepeau, and J.H. Freed, J. Magn. Reson. **127** (2), 155 (1997).
[18] G.A. Rinard, R.W. Quine, J.R. Harbridge, R.T. Song, G.R. Eaton, and S.S. Eaton, J. Magn. Reson. **140** (1), 218 (1999).
[19] D.I. Hoult, Concept Magnetic Res **12** (4), 173 (2000).
[20] J. Krupka, R.G. Geyer, M. Kuhn, and J.H. Hinken, IEEE Trans. Microwave Theory Techniques **42** (10), 1886 (1994).
[21] L. Fan, M.Y. Li, and K. Chang, Electron. Lett. **31** (4), 294 (1995).
[22] J. Forrer, I. Garcia-Rubio, R. Schuhmam, R. Tschaggelar, and J. Harmer, J. Magn. Reson. **190** (2), 280 (2008).
[23] J.W. Sidabras, R.R. Mett, W. Froncisz, T.G. Camenisch, J.R. Anderson, and J.S. Hyde, Rev. Sci. Instrum. **78** (3), (2007).
[24] P.P. Borbat and J.H. Freed, in *Biological Magnetic Resonance, Vol. 19, Distance Measurements in Biological Systems by EPR*, edited by L.J. Berliner, G.R. Eaton, and S.S. Eaton (Academic Press, New York, 2000).
[25] H. Yagi, D. Banerjee, B. Graham, T. Huber, D. Goldfarb, and G. Otting, J. Am. Chem. Soc. **133** (27), 10418 (2011).
[26] A. Blank, Y. Talmon, M. Shklyar, L. Shtirberg, and W. Harneit, Chem. Phys. Lett. **465** (1–3), 147 (2008).